



## Computational Modeling of Coronary Artery Flow and Pressure: A CFD Approach for Cardiovascular Disease Dynamic

<sup>1</sup>Sani Usman, <sup>2</sup>Mohammed Abdulhameed, <sup>3</sup>M. S. Adamu, <sup>4</sup>Abdulsalam Y. Gital

<sup>1</sup>Department of Computer Science

<sup>2</sup>Department of Mathematics and Statistics

Federal Polytechnic Bauchi

<sup>3</sup>Department of Mathematical Sciences

<sup>4</sup>Department of Computer Science,

Abubakar Tafawa Balewa University, Bauchi

### ABSTRACT

*This research paper presents a computational fluid dynamics (CFD) approach to modeling pulsating blood flow with magnetic particles through a stenosed artery under the influence of an applied magnetic field, oscillating pressure gradient, external body acceleration, and slip velocity. A mathematical model was developed to describe the coupled dynamics of blood and magnetic particles, and the governing equations were solved analytically and simulated using MATHCAD software. Key findings indicate that blood velocity and magnetic particle velocity can be modulated by adjusting the magnetic parameter. In the absence of stenosis, blood flow remains constant along the axial coordinate. However, within the stenosed region, significant variations in blood velocity occur, with peak velocity and shear stress observed at the throat of the stenosis. Notably, shear stress is higher near the artery's longitudinal axis in stenosed areas, while it remains relatively constant in non-stenosed regions. The study underscores the potential of CFD modeling in understanding complex hemodynamic behavior within stenosed arteries. By incorporating magnetic fields and external influences, the model provides valuable insights into blood flow regulation, which could benefit cardiovascular diagnostics and treatment strategies. The ability to control blood and particle velocities through magnetic parameters suggests promising applications in targeted drug delivery and non-invasive therapeutic interventions. Future research could refine the model further by incorporating patient-specific data and exploring real-time clinical applications.*

### ARTICLE INFO

Article History

Received: August, 2024

Received in revised form: August, 2024

Accepted: September, 2024

Published online: December, 2024

### KEYWORDS

Coronary artery, Stenosed artery,  
Differential model, Analytical solutions

### INTRODUCTION

Heart disease is the leading cause of death in the world and is principally caused by atherosclerosis in the coronary arteries which provide blood supply to the heart muscle. Patient-specific computational models of blood flow in the coronary arteries have emerged in recent years as a clinically important technology to aid in the diagnosis and treatment of heart disease [1]. The use of patient-specific models of blood flow in

coronary arteries is supported by robust clinical data demonstrating accuracy against direct, invasive measures [2–5] and safety, efficacy and cost-effectiveness when introduced into clinical care [6–10].

Patient-specific computational models of coronary artery blood flow incorporate mathematical models of blood flow in arteries [11–13]. Any mathematical model of blood flow in the circulation includes at least three elements: first, a

Corresponding author: Mohammed Abdulhameed

✉ [amohd@fptb.edu.ng](mailto:amohd@fptb.edu.ng)

Department of Mathematics and Statistics, Federal Polytechnic Bauchi.

© 2024. Faculty of Technology Education. ATBU Bauchi. All rights reserved



geometric description of the anatomic region of interest; second, the mathematical “governing equations” enumerating the physical laws of blood flow within the region of interest; and, third, “boundary conditions” to define physiologic relationships between variables at the boundaries of the region of interest. While the anatomic region of interest and the boundary conditions are unique to each patient and the specific vascular territory, the governing equations describing velocity and pressure are universal and apply in different patients and other arterial beds.

Patient-specific models of coronary artery blood flow can be used to predict outcomes of coronary artery revascularization procedures, to identify patients at risk of having a heart attack, and to model tissue perfusion of the microcirculation by coupling with emerging models of cardiac function. In this research work, we provide a state-of-the-art computational method for, and applications of, quantifying blood flow in patient-specific models of the coronary arteries.

According to the previous research, the blood flow issue has been divided into two characters, namely, Newtonian and non-Newtonian fluid. Following various blood models, the impacts of artery wall elasticity, flow of blood with heat transfer, fluid particle transport are investigated [14–16]. Since blood consists of blood cells and plasma and generally approaches as a Newtonian fluid. Nevertheless, in accordance with the blockage artery conditions, blood should be considered as a non-Newtonian nature [17]. Though doctors use diagnostic parameters as a practical purpose, the application has not been well established in early studies. The general diagnostic parameters [18,19] are fractional flow reserve (FFR), pressure drop coefficient (CDP) and lesion flow coefficient (LFC) which have common application. Numerical simulations of an oscillating flow past in the conduits of plane through the wall obstacles of the square have been reported by investigator [20]. Such outcomes are of eminent gusto as the pulsatile flow area is employed. Liao et al. [21] have studied a bell-shaped constriction for three various patterns of flows of pulsation and decided that the perturbations of characteristic flow parameters

influence the flow area in case of physiological flow. Halder et al. [22] have discussed the comparative analysis between Newtonian and non-Newtonian fluids through a stenotic vessel. Razavi et al. [23] have numerically investigated the flow dynamics through an axisymmetric common carotid stenotic artery varying blockage intensity 30-60% under Newtonian and non-Newtonian blood rheological models.

A numerical investigation may have great impacts on the essentiality of applying patient-specific inflow velocity profiles to examine the thoracic aorta disease states using finite element method [24]. In 3D bifurcated carotid artery, the hemodynamic changes have been investigated for the bifurcation angle of symmetric and asymmetric due to steady and pulsatile flow. The simulated results reveal the significant difference in behavior between steady and pulsatile flow [25]. Lakzian et al. [26] have studied the Newtonian and non-Newtonian unsteady blood pulsatile flow in a 3D curved stenotic artery. The findings point out that the maximum wall shear stress occurs at the neck of the blockage. Abbas et al. [27] have numerically investigated the pulsatile blood flow through an arterial overlapping stenotic blood vessel under the action of periodic body acceleration. The Sutterby fluid model characterizes the blood rheology. The software, COMSOL Multiphysics [28] is used for solving the set of governing equations, subject to the corresponding boundary conditions.

Hence, in the present research, the most well-known blood constitutive equation namely, the Carreau model as a non-Newtonian fluid has been activated in an attempt to examine the blood pulsatile flow through the stenotic and bifurcated left coronary artery. A numerical model of arterial blood flow is induced for two-dimensional (2D) and 3D bifurcated geometry to give the idea about the hemodynamic changes, to provide clinical diagnosis treatment and to establish a comparison between Newtonian and non-Newtonian fluid. The non-Newtonian importance factor has also provided a new concept for arterial flows.

Despite advances in CAD diagnostics, existing methods often lack accuracy in non-

---

Corresponding author: Mohammed Abdulhameed

✉ [amohd@fptb.edu.ng](mailto:amohd@fptb.edu.ng)

Department of Mathematics and Statistics, Federal Polytechnic Bauchi.

© 2024. Faculty of Technology Education. ATBU Bauchi. All rights reserved

invasively assessing coronary artery health. Computational models of coronary artery hemodynamics are underutilized in clinical settings, due to the complexity of creating accurate simulations that reflect patient-specific conditions. This proposal seeks to address this gap by developing a CFD-based model capable of simulating coronary artery flow and pressure, potentially improving diagnostic accuracy and treatment outcomes

### Formulation of the problem

The model formulation of the problem involves the application of computational fluid dynamics (CFD) to simulate blood flow and pressure within a coronary artery, specifically under conditions of stenosis (narrowing of the artery). The formulation is designed to analyze the fluid behavior, including non-Newtonian characteristics, pulsatile flow, and the influence of external forces such as magnetic fields and body acceleration.

The model is structured around several key components that define the blood flow dynamics in a coronary artery. Firstly, the artery geometry is represented through realistic models, including Figure 1(a), which illustrates the human coronary artery, Figure 1(b) showing the left coronary bifurcation, and Figure 2 depicting a stenosed artery, where narrowing affects the flow

dynamics. The stenosis model accounts for the artery's narrowing along the axial coordinate, with severity varying along the artery's length and mathematically described by Equation 1. Blood is modeled as a non-Newtonian fluid using the Bingham plastic model, which incorporates blood's yield stress and its inability to flow until a certain threshold of applied stress is surpassed. This non-Newtonian behavior is crucial for accurately simulating blood flow, especially under varying flow rates and stresses. The model also includes an applied magnetic field that affects the behavior of magnetic particles suspended in the blood, which are assumed to be uniformly distributed and interact with both the fluid and magnetic field along the artery's axis. The flow conditions are characterized by pulsatile blood flow, with a cyclic variation in response to the heart's pumping action, along with an oscillating pressure gradient along the artery's axial direction. Additionally, periodic body acceleration is considered to account for the impact of external forces like body movement or respiration on the flow dynamics. Lastly, a slip velocity is assumed at the stenosed wall, meaning that the fluid near the wall does not adhere strictly to it, allowing for slip-like behavior in constricted regions, which is an important factor in regions with turbulent or high-shear flow.

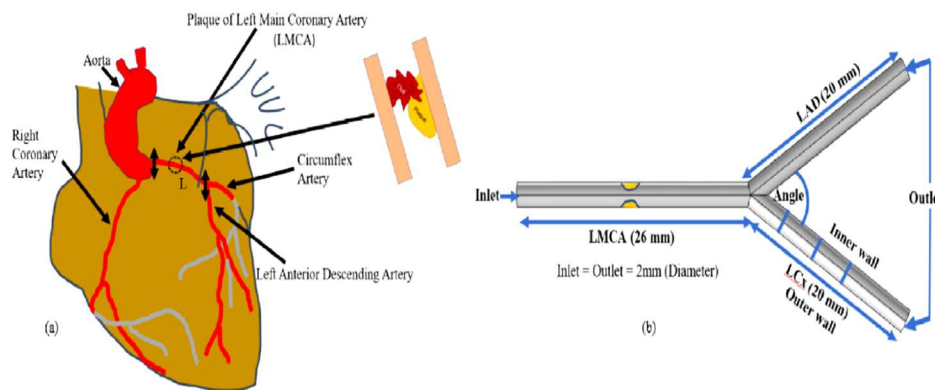


Figure 1: (a) Human realistic coronary artery (b) Left coronary bifurcation model used in the study

Corresponding author: Mohammed Abdulhameed  
 ✉ [amohd@fptb.edu.ng](mailto:amohd@fptb.edu.ng)  
 Department of Mathematics and Statistics, Federal Polytechnic Bauchi.  
 © 2024. Faculty of Technology Education. ATBU Bauchi. All rights reserved

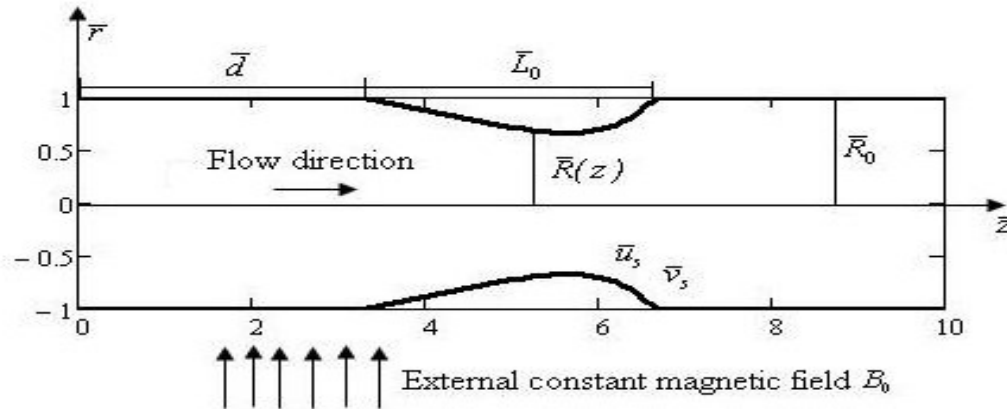


Fig. 2 Geometry of stenosis

$$\frac{\bar{R}(z)}{\bar{R}(0)} = \begin{cases} 1 - \bar{\psi} \left[ \bar{L}_0^{-1} (\bar{z} - \bar{d}) - (\bar{z} - \bar{d})^m \right], & \bar{d} \leq \bar{z} \leq \bar{d} + \bar{L}_0 \\ 1, & \text{otherwise} \end{cases} \quad (1)$$

Where

$\bar{R}(\bar{z})$  is the radius of the artery in the stenosed region,

$\bar{R}(0) = \bar{R}_0$  is the radius of the normal artery,

$\bar{L}_0$  is the length of the stenosis,

$\bar{d}$  is the region of the stenosis and

$\bar{\psi} = \left( \frac{\xi_s}{\bar{R}(0)\bar{L}_0^m} \right) \frac{m^{m/(m-1)}}{(m-1)}$  is the maximum

height of the stenosis at  $\bar{z} = \bar{d} + (\bar{L}_0 / m^{m/(m-1)})$  such that

$$\xi_s / \bar{R}(0) < 1.$$

The considered model for the blood motion consists of Navier-Stokes equations, the constitutive equations of the Bingham plastic fluid and the following Maxwell's equations of the magnetic field:

$$\nabla \cdot \mathbf{B} = 0, \nabla \times \mathbf{B} = \mu_0 \mathbf{J}, \nabla \times \mathbf{E} = -\frac{\partial \mathbf{B}}{\partial t}, \quad (2)$$

where  $\mathbf{B}$  is the magnetic flux intensity,  $\mu_0$  is the magnetic permeability,  $\mathbf{E}$  is the electric field intensity and  $\mathbf{J}$  is the current density given by  $\mathbf{J} = \sigma(\mathbf{E} + \mathbf{v} \times \mathbf{B})$ ,

$\sigma$  being the electrical conductivity and  $\mathbf{v}$  is the velocity field

The electromagnetic body force  $\mathbf{F}_{em}$  is defined as

$$\mathbf{F}_{em} = \mathbf{J} \times \mathbf{B} = \sigma(\mathbf{E} + \mathbf{v} \times \mathbf{B}) \times \mathbf{B} = \sigma B_0^2 \bar{u}(r, t) \mathbf{k}, \quad (4)$$

where  $\mathbf{k}$  is the unite vector of the  $z$ -direction

and  $\mathbf{v} = \bar{u}(r, t) \mathbf{k}$  is the axial velocity of the

blood. The electromagnetic body force  $\mathbf{F}_{em}$  is inserted in the momentum Eq. (5).

In the assumption that the ratio of the maximum height of the stenosis and the radius of the non-stenotic region, respectively, the ratio of the radius of non-stenotic region and the length of stenosis are much smaller than the unity, the governing equation of motion and stress tensor are given by<sup>[23]</sup>:

#### Momentum equation

$$\rho \left( \frac{\partial \bar{u}}{\partial t} \right) = - \left( \frac{\partial \bar{p}}{\partial z} \right) - \left( \frac{1}{r} \right) \frac{\partial}{\partial r} (r\tau) + \bar{G}(t) + KN(\bar{v} - \bar{u}) - \sigma B_0^2 \bar{u}, \quad (5)$$

The constitutive Bingham plastic model

stress tensor  $\bar{\tau}$  of the form<sup>[10]</sup>

$$\bar{\tau} = \bar{\tau}_y - \mu \left( \frac{\partial \bar{u}}{\partial r} \right); \text{ for } \bar{\tau} \geq \bar{\tau}_y \quad (6)$$

$$\frac{\partial \bar{u}}{\partial r} = 0, \quad \text{for } \bar{\tau} < \bar{\tau}_y \quad (7)$$

where  $\bar{u}$  is the axial velocity of blood,  $\bar{v}$  is the velocity of particles,  $\bar{t}$  is the time,  $\bar{p}$  is the pressure,  $\bar{\tau}$  is the shear stress,  $\bar{G}(\bar{t})$  is the body acceleration,  $B_0$  is the externally applied

constant magnetic field,  $\bar{\sigma}_y$  is the yield stress,  $\rho$  is the density of blood,  $\mu$  is the dynamic viscosity of the blood,  $K$  is the Stokes constant,  $N$  is the number of magnetic particles per unit

volume and  $\frac{KN}{\rho}(\bar{v} - \bar{u})$  is the interaction between motion of blood and magnetic particles. We considered the Reynolds number of the relative velocity is small; therefore the force between blood and magnetic particles is proportional to the relative velocity.

The periodic body acceleration  $\bar{G}(\bar{t})$  and pressure gradient  $\frac{\partial \bar{p}}{\partial z}(\bar{z}, \bar{t})$  for  $\bar{t} > 0$ , which appears in Eq. (5), have the expression of the following forms<sup>[10]</sup>:

$$\bar{G}(\bar{t}) = B_0 \cos(\omega_b \bar{t} + \varphi), \quad (8)$$

$$-\frac{\partial \bar{p}}{\partial z}(\bar{z}, \bar{t}) = A_0 + A_1 \cos(\omega_p \bar{t}), \quad (9)$$

where  $\omega_b = 2\pi \bar{f}_b$  is the frequency,  $\bar{f}_b$  is the pulse rate frequency,  $\varphi$  is the lead angle of the body acceleration with respect to the pressure gradient,  $\omega_p = 2\pi \bar{f}_p$  is the heart pressure

frequency,  $\bar{f}_p$  is the pulse rate frequency,  $A_0$  is the amplitude of the steady state pressure gradient, and  $A_1$  is the amplitude of the oscillating pressure gradient.

The motion of nanoparticles in the vascular system is governed by a number of forces<sup>[16]</sup>. In the current investigation, we consider the fluidic force and the unsteady flow analysis are implemented. Therefore, the motion of magnetic single particle is governed by Newton's law for dynamic of particle motion

$$M \frac{\partial \bar{v}}{\partial t} = \sum F_{\text{ext}}, \quad (10)$$

where  $M$  is the mass of the single nanoparticles and  $\sum F_{\text{ext}} = F_m + F_b + F_{\text{blood}}$  represents all the external forces exerted on the particle from which  $F_m$  is the magnetic force,  $F_b$  is the buoyancy force and  $F_{\text{blood}}$  is the fluidic force. The fluidic force experience by a particle, assuming a Reynolds number  $\text{Re} \leq 1$ , is predicted using Stokes's law for viscous drag on a sphere

$$F_{\text{blood}} = -6\pi\mu E_{\text{hyd,p}}(\bar{v} - \bar{u}), \quad (11)$$

where  $E_{\text{hyd,p}}$  is the effective hydrodynamic radius of the particle,  $\bar{v}$  is the particle velocity, the  $\ominus$  sign indicates that the fluidic force acts opposite to the direction of the particles motion. We predict particle motion when only the force on the particle is fluidic and no buoyancy force

$$M \frac{\partial \bar{v}}{\partial t} = K(\bar{u} - \bar{v}), \quad (12)$$

where  $K = 6\pi\mu E_{\text{hyd,p}}$  is the Stokes's constant.

## 2.2 Initial and boundary conditions

To the proposed problem, we consider the following initial and boundary condition

$$\bar{u} = \bar{v} = 0, \quad \text{at } \bar{t} = 0, \quad (13)$$

$$\bar{u} = \bar{u}_s \text{ and } \bar{v} = \bar{v}_s \text{ at } \bar{r} = \bar{R}(z), \quad (14)$$

$$\bar{\tau} \text{ is finite, at } \bar{r} = 0, \quad (15)$$

where  $\bar{u}_s, \bar{v}_s$  are the slip velocities at the stenotic walls (see Fig. 1)

The dimensionless forms of the governing equations are obtained by considering the following dimensionless variables:

$$u = \frac{\bar{u}}{A_0 \bar{R}_0 / 4\mu}, \quad v = \frac{\bar{v}}{A_0 \bar{R}_0 / 4\mu}, \quad \theta = \frac{\bar{\tau}_y}{A_0 \bar{R}_0 / 2}, \quad R(z) = \frac{\bar{R}(z)}{\bar{R}_0}$$

$$t = \bar{t} w_p, \quad A = \frac{A_1}{A_0}, \quad \xi_s = \frac{\bar{\xi}_s}{\bar{R}_0}, \quad B = \frac{B_0}{A_0}, \quad r = \frac{\bar{r}}{\bar{R}_0},$$

$$u_s = \frac{\bar{u}_s}{A_0 \bar{R}_0 / 4\mu}, \quad v_s = \frac{\bar{v}_s}{A_0 \bar{R}_0 / 4\mu}, \quad \omega = \frac{\bar{\omega}_b}{w_p}, \quad \tau = \frac{\bar{\tau}}{A_0 \bar{R}_0 / 2}. \quad (16)$$

Eqs. (5), (12) and (7) becomes:

$$\alpha^2 \frac{\partial u}{\partial t} = f(t) + R_1(v-u) - \frac{2}{r} \frac{\partial}{\partial r}(r\tau) - Ha^2 u, \quad (17)$$

$$\alpha^2 \frac{\partial v}{\partial t} = \frac{1}{G}(u-v), \quad (18)$$

$$\tau = \theta - \frac{1}{2} \frac{\partial u}{\partial r}; \quad \text{for } \tau \geq \theta \quad (19)$$

$$\frac{\partial u}{\partial r} = 0, \quad \text{for } \tau < \theta \quad (20)$$

The dimensionless initial and boundary conditions are:

$$u = v = 0, \quad \text{at } t = 0, \quad (21)$$

$$u = u_s, \quad v = v_s, \quad \text{at } r = R(z) \quad (22)$$

$$\tau \text{ is finite, at } r = 0, \quad (23)$$

where  $\alpha^2 = \frac{\bar{w}_p \bar{R}_0^2 \rho}{\mu}$  is the Womersley

frequency parameter,  $Ha = \sqrt{\frac{\sigma}{\mu}} B_0 \bar{R}_0$  is the

Hartmann number,  $R_1 = \frac{KN \bar{R}_0^2}{\mu}$  is the particle

$$G = \frac{M\mu}{\rho \bar{R}_0^2 K}$$

concentration parameter,  $\frac{M\mu}{\rho \bar{R}_0^2 K}$  is the particle mass parameter and  $f(t) = 4[(1 + A \cos t) + B \cos(\omega t + \phi)]$ ,

It is important to point out that, if the particle concentration parameter is zero ( $R_1 = 0$ ) and no magnetic field effect ( $Ha = 0$ ), then Eq. (17) represent the classical model which was given by [10].

### Solution of the problem

Let the blood velocity  $u$ , the magnetic particles velocity  $v$  and the shear stress  $\tau$  expressed in the forms:

$$u(z, r, t) = u_0(z, r, t) + \alpha^2 u_1(z, r, t) + \dots \quad (24)$$

$$\tau(z, r, t) = \tau_0(z, r, t) + \alpha^2 \tau_1(z, r, t) + \dots \quad (25)$$

$$v(z, r, t) = v_0(z, r, t) + \alpha^2 v_1(z, r, t) + \dots \quad (26)$$

Substituting  $u, v$  and  $\tau$  from Eqs. (24)-(26) into Eqs. (17)-(19) and equating the coefficients of  $\alpha^0$  and  $\alpha^2$ , respectively, we obtained:

$$f(t) + R_1(v_0 - u_0) - Ha^2 u_0 - \frac{2}{r} \frac{\partial}{\partial r}(r\tau_0) = 0, \quad (27)$$

$$u_0 - v_0 = 0, \quad (28)$$

$$\tau_0 = \theta - \frac{1}{2} \frac{\partial u_0}{\partial r}. \quad (29)$$

and

$$\frac{\partial u_0}{\partial t} = R_1(v_1 - u_1) - Ha^2 u_1 - \frac{2}{r} \frac{\partial}{\partial r}(r\tau_1), \quad (30)$$

$$G \frac{\partial v_0}{\partial t} = u_1 - v_1, \quad (31)$$

$$\tau_1 = -\frac{1}{2} \frac{\partial u_1}{\partial r}. \quad (32)$$

Substituting Eqs. (28) and (29) into Eq. (27), we obtain

$$\frac{2}{r} \frac{\partial}{\partial r} \left[ r \left( \theta - \frac{1}{2} \frac{\partial u_0}{\partial r} \right) \right] + Ha^2 u_0 - f(t) = 0, \quad (33)$$

Making the change of function

$$Ha^2 u_0 - f(t) = 2F_0(r, z, t), \quad (34)$$

Eq. (33) becomes

$$r \frac{\partial^2 F_0}{\partial r^2} + \frac{\partial F_0}{\partial r} - Ha^2 r F_0 = \theta Ha^2. \quad (35)$$

We seek the solution of Eq. (35) in the form of power series as

$$F_0 = \sum_{n=0}^{\infty} C_n(z, t) r^n. \quad (36)$$

It follows that, the general terms for  $C_{2n+1}$  and  $C_{2n+2}$  can be immediately followed, respectively as:

$$C_{2n+1} = (2Ha)^{2n} \left( \frac{n!}{(2n+1)!} \right)^2 C_1 = (2Ha)^{2n} \left( \frac{n!}{(2n+1)!} \right)^2 \theta Ha^2, \quad (37)$$

$$C_{2n+2} = \left( \frac{Ha}{2} \right)^{2(n+1)} \frac{C_0}{[(n+1)!]^2} \quad n=0, 1, 2, \dots, \quad (38)$$

The function  $F_0(r, z, t)$  is expressed as:

$$\begin{aligned} F_0(r, z, t) &= C_0 + \sum_{n=0}^{\infty} C_{2n+1} r^{2n+1} + \sum_{n=0}^{\infty} C_{2n+2} r^{2n+2} \\ &= C_0 + \theta Ha^2 \sum_{n=0}^{\infty} (2Ha)^{2n} \left( \frac{n!}{(2n+1)!} \right)^2 r^{2n+1} \\ &\quad + C_0 \sum_{n=0}^{\infty} \left( \frac{Ha}{2} \right)^{2(n+1)} \frac{r^{2n+2}}{[(n+1)!]^2}, \end{aligned} \quad (39)$$

which can be written in the simpler form

$$r \frac{\partial^2 u_1}{\partial r^2} + \frac{\partial u_1}{\partial r} - Ha^2 u_1 r = \left[ 1 - \sum_{n=0}^{\infty} \left( \frac{Ha}{2} \right)^{2(n+1)} \frac{r^{2n+2}}{[(n+1)!]^2} \right] h(t) r, \quad (45)$$

where

$$h(t) = \frac{4(1+RG)}{Ha^2} \frac{df(t)}{dt}. \quad (46)$$

$$F_0(r, z, t) = C_0(z, t) I_0(H_a r) + \frac{\pi \theta}{2} \sum_{n=0}^{\infty} \frac{1}{[\Gamma(n + \frac{3}{2})]^2} \left( \frac{r H_a}{2} \right)^{2n+1}. \quad (40)$$

The solution  $u_0$  can be expressed as

$$u_0 = \frac{2F_0(r, z, t) + f(t)}{Ha^2}. \quad (41)$$

Using the boundary condition  $u_0 = u_s$  at  $r = R(z)$ , we obtain

$$C_0(z, t) = \frac{1}{2} \left[ \frac{Ha^2 u_s - f(t) - \pi \theta Ha^2 b(z)}{I_0(H_a R(z))} \right], \quad (42)$$

$$b(z) = \sum_{n=0}^{\infty} \frac{1}{[\Gamma(n + \frac{3}{2})]^2} \left[ \frac{H_a R(z)}{2} \right]^{2n+1}$$

with

and  $I_0$  is the modified Bessel function of order zero.

The solution of  $v_0$  and  $\tau_0$  can be readily expressed as

$$v_0 = u_0, \quad (43)$$

$$\tau_0 = \theta - \frac{1}{Ha^2} \frac{\partial F_0(r, z, t)}{\partial r}. \quad (44)$$

Following the same procedure for obtaining  $u_0$ ,  $v_0$  and  $\tau_0$ , the  $u_1$ ,  $v_1$  and  $\tau_1$  can be achieved similarly.

Substituting Eqs. (31) and (32) into Eq. (30), we obtain:

The solution of the problem (45), (46) with the boundary condition  $u_1(R(z), z, t) = 0$  is

$$u_1(r, z, t) = \frac{h(t)}{4} r^2 + D_0(z, t) + D_0(z, t) \sum_{n=1}^{\infty} \left( \frac{Ha}{2} \right)^{2n+2} \frac{r^{2n+2}}{((n+1)!)^2} + \sum_{n=1}^{\infty} D_{2n+1} r^{2n+1}, \quad D_0 = - \frac{\frac{h(t)}{4} R^2(z) + \sum_{n=1}^{\infty} D_{2n+1} R^{2n+1}(z)}{1 + \sum_{n=0}^{\infty} \left( \frac{Ha}{2} \right)^{2n+2} \frac{R^{2n+2}(z)}{((n+1)!)^2}}. \quad (47)$$

The solution of  $v_1$  and  $\tau_1$  are immediately follow as

$$v_1 = u_1 - G \frac{\partial v_0}{\partial t}, \quad \tau_1 = - \frac{1}{2} \frac{\partial u_1}{\partial r}. \quad (48)$$

The above obtained solution represents an approximate solution and it was determined under assumption that the Womersley number  $\alpha$  has small values. This is a very restrictive condition. In

$$u(z, r, t) = u_s - \frac{2u_s}{R(z)} \sum_{n=1}^{\infty} \frac{J_0(r r_n(z))}{r_n(z) J_1(R(z) r_n(z))} M_n(z, t) + \frac{2}{R^2(z)} \sum_{n=1}^{\infty} \frac{J_0(r r_n(z))}{J_1^2(R(z) r_n(z))} \int_0^t N_n(z, \tau) S_n(z, t - \tau) d\tau, \quad (49)$$

where,

$$M_n(z, t) = 1 - \frac{\alpha^2 G r_n^2(z) q_{1n}(z) + r_n^2(z) e^{q_{1n}(z)t} - 1}{\alpha^4 G (q_{1n}(z) - q_{2n}(z)) q_{1n}(z)} + \frac{\alpha^2 G r_n^2(z) q_{2n}(z) + r_n^2(z) e^{q_{2n}(z)t} - 1}{\alpha^4 G (q_{1n}(z) - q_{2n}(z)) q_{2n}(z)}, \quad (50)$$

$$N_n(z, t) = \frac{\alpha^2 G q_{1n}(z) + 1}{\alpha^4 G (q_{1n}(z) - q_{2n}(z))} e^{q_{1n}(z)t} - \frac{\alpha^2 G q_{2n}(z) + 1}{\alpha^4 G (q_{1n}(z) - q_{2n}(z))} e^{q_{2n}(z)t}, \quad (51)$$

$$S_n(z, t) = 4 \rho_n(z) (1 + A \cos(t) + B \cos(\omega t + \varphi)) + \sigma_n(z), \quad (52)$$

$$\rho_n(z) = \frac{R(z)}{r_n(z)} J_1(R(z) r_n(z)), \quad \sigma_n(z) = -2\theta \int_0^{R(z)} J_0(r r_n(z)) dr \quad (53)$$

Corresponding author: Mohammed Abdulhameed

✉ [amohd@fptb.edu.ng](mailto:amohd@fptb.edu.ng)

Department of Mathematics and Statistics, Federal Polytechnic Bauchi.

© 2024. Faculty of Technology Education. ATBU Bauchi. All rights reserved

$$q_{1n}(z), q_{2n}(z) = \frac{-\left(1 + G(R + Ha^2 + r_n^2(z))\right) \pm \sqrt{\left[1 + G(R + Ha^2 + r_n^2(z))\right]^2 - 4G(Ha^2 + r_n^2(z))}}{2\alpha^2 G}, \quad (54)$$

and  $r_n(z)$  are the positive roots of the transcendental equation  $J_0(R(z)r_n) = 0$ .

### ANALYSIS OF RESULTS AND DISCUSSION

We have investigated the mathematical model that represents the non-Newtonian flow of blood through a stenosed artery in the presence of an external magnetic field perpendicular to the flow direction. A periodic body acceleration and an oscillating pressure gradient along the flow direction are considered using a time-periodic function (Fig. 2). Under the assumption of small values of the Womersley number, approximate solutions to the axial velocity of fluid and suspended particles, as well as to the shear stress, were determined. Numerical calculations were performed using MATHCAD software to analyze flow parameters. The computed results are illustrated in Figs. 3-5 to provide quantitative estimates.

Figures 3 and 4 depict the variation of dimensionless axial velocity with the axial coordinate for different values of the Hartmann number and time. As expected, in the absence of zstenosis, axial blood velocity remains constant at each instant and in each circular fluid layer. However, in the stenosed region, significant velocity variations occur. The fluid velocity increases slightly in the stenotic area but rises significantly at the maximum stenosis height, where the orifice diameter is smallest. Additionally, an increase in the Hartmann number (stronger magnetic field) results in a substantial variation in axial velocity. Lower Hartmann numbers lead to higher maximum fluid velocity due to the reduced influence of the Lorentz force, which opposes the motion of the electrically conducting fluid. The externally applied transverse magnetic field effectively decelerates blood flow. Figure 5 illustrates the impact of different Hartmann numbers, radial positions, and axial positions on shear stress within the stenosed artery. The results indicate that shear stress

consistently decreases in the presence of a stronger magnetic field. Peak shear stress is observed at the throat of the stenosis, highlighting its significance in arterial wall deterioration. The shear stress distribution plays a crucial role as the generation of tension on arterial walls is linked to potential damage.

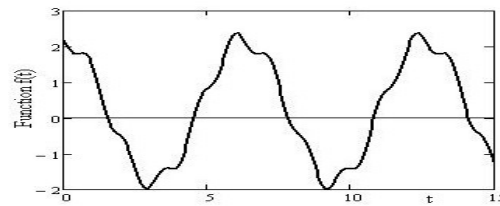


Fig. 2. Function  $f(t)$  – the oscillating pressure gradient and body acceleration

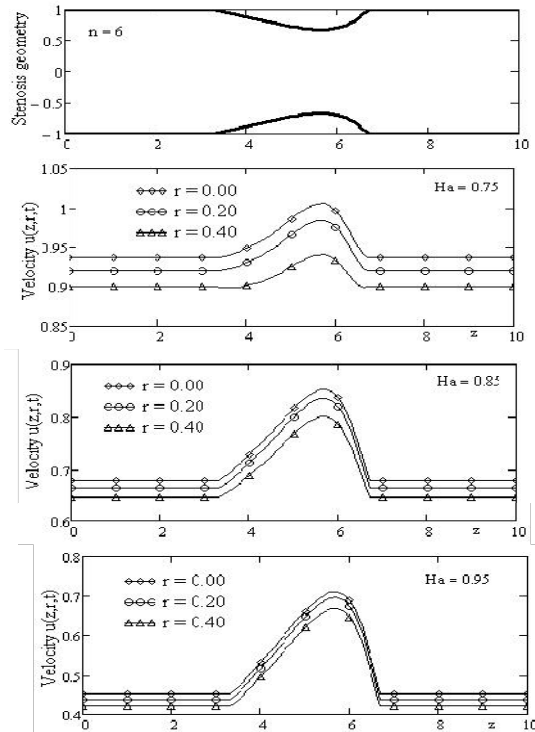


Fig. 3. Profiles of the axial velocity  $u(z,r,t)$  for time  $t = 1$  and for different values of Hartman number  $Ha$

Corresponding author: Mohammed Abdulhameed

✉ [amohd@fpb.edu.ng](mailto:amohd@fpb.edu.ng)

Department of Mathematics and Statistics, Federal Polytechnic Bauchi.

© 2024. Faculty of Technology Education. ATBU Bauchi. All rights reserved

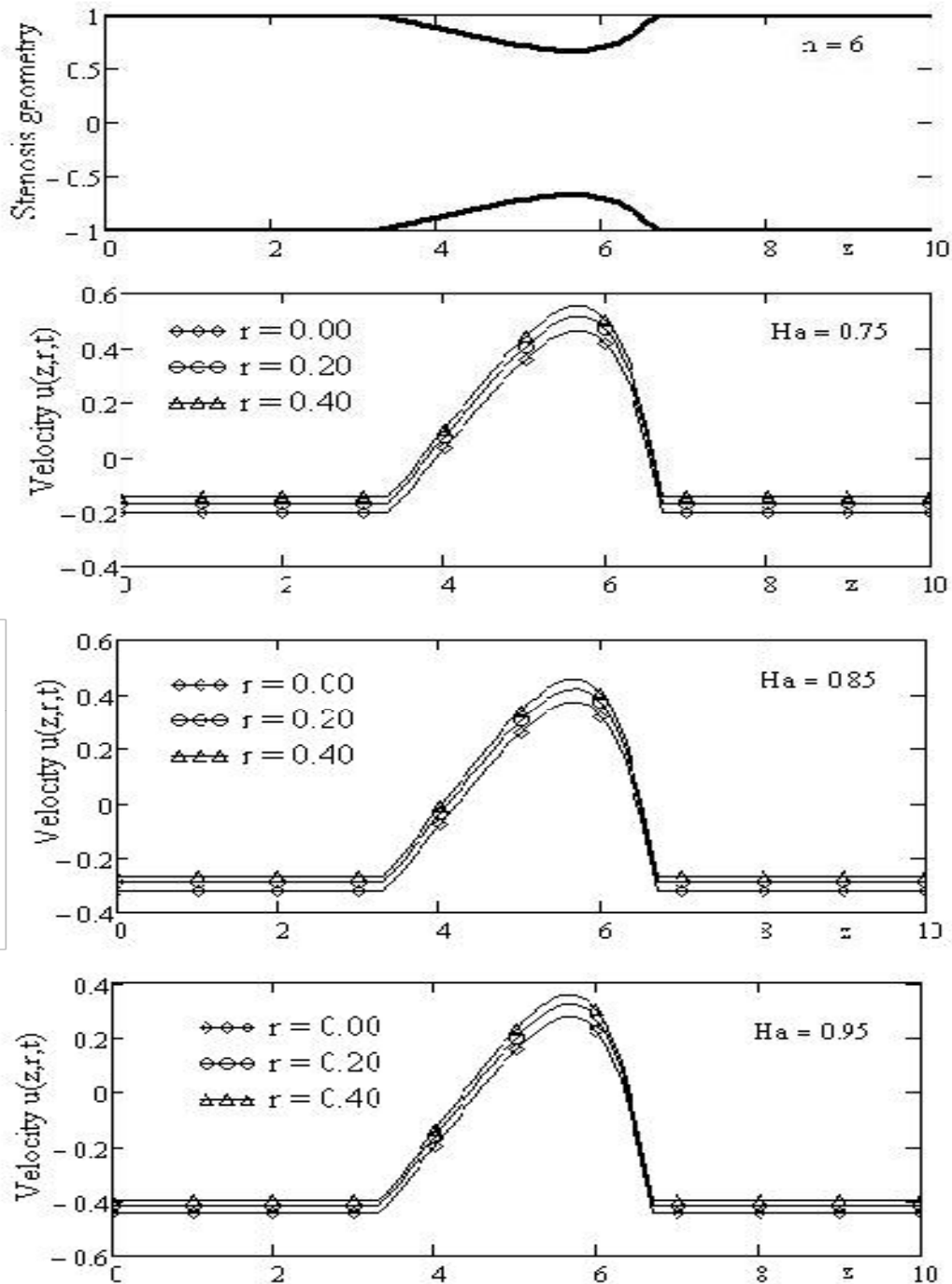


Fig. 4. Profiles of the axial velocity  $u(z,r,t)$  for time  $t = 4$  and for different values of Hartman number  $Ha$

Corresponding author: Mohammed Abdulhameed  
 ✉ [amohd@fpb.edu.ng](mailto:amohd@fpb.edu.ng)  
 Department of Mathematics and Statistics, Federal Polytechnic Bauchi.  
 © 2024. Faculty of Technology Education, ATBU Bauchi. All rights reserved

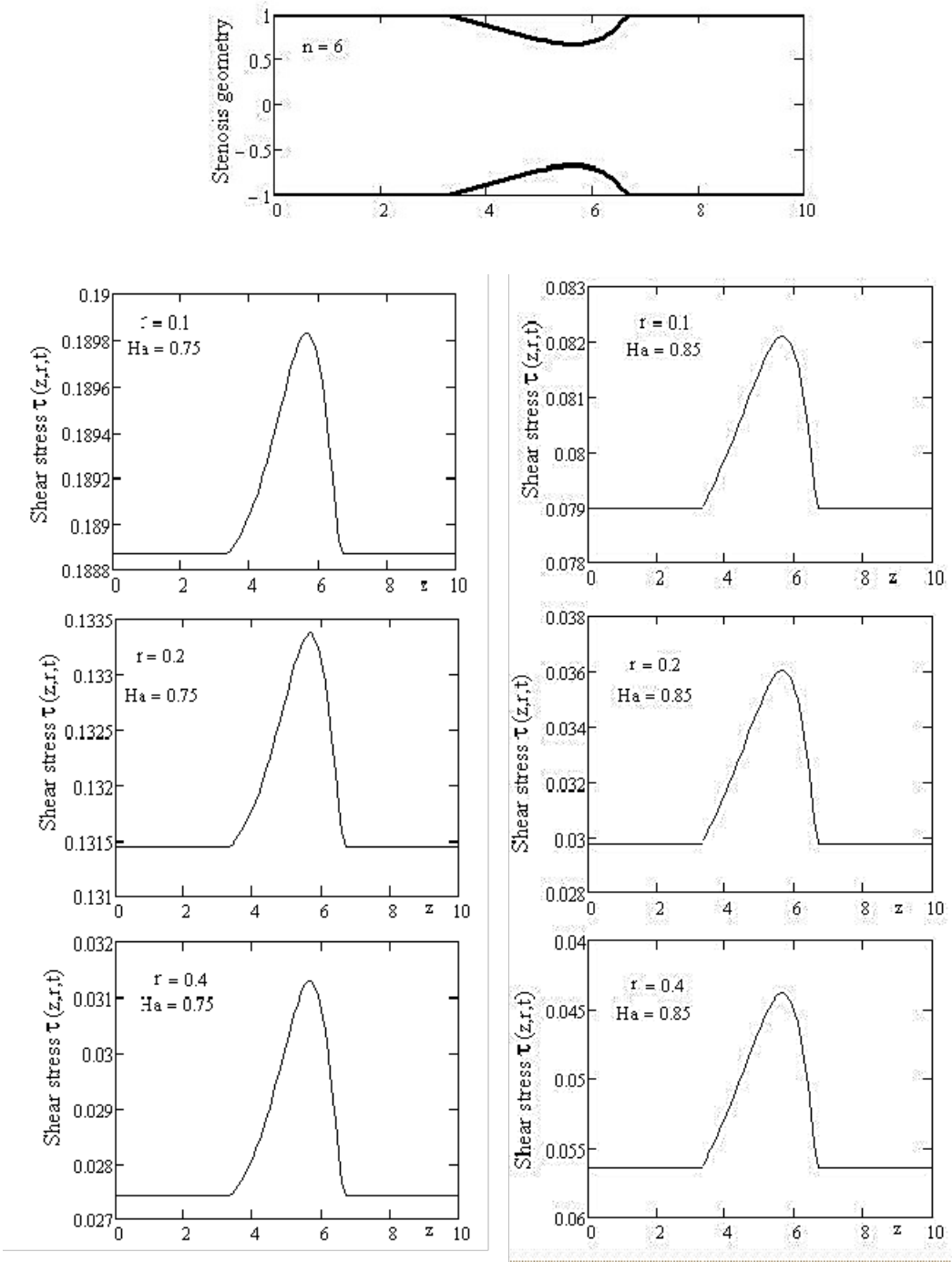


Fig. 5. Profiles of the shear stress  $\tau(z,r,t)$  for time  $t = 1$ ,  $\nu = 0.75$  and for different values of Hartman number  $Ha$

Corresponding author: Mohammed Abdulhameed  
 ✉ [amohd@fptb.edu.ng](mailto:amohd@fptb.edu.ng)  
 Department of Mathematics and Statistics, Federal Polytechnic Bauchi.  
 © 2024. Faculty of Technology Education, ATBU Bauchi. All rights reserved



## CONCLUSION

This research presents a mathematical model that describes pulsating blood flow and magnetic particles through a stenosed artery under various conditions, including a magnetic field, oscillating pressure gradient, external body acceleration, and slip velocity. The study finds that blood and magnetic particle velocities can be controlled by adjusting the magnetic parameter, and that in non-stenosed areas, blood flow remains constant, while significant velocity variations occur in stenosed areas. The shear stress is constant in non-stenosed regions but much higher in stenosed areas, with peak velocity and shear stress occurring at the stenosis throat. CFD simulations reveal disturbed flow patterns, elevated wall shear stress in stenosed arteries, and significant pressure drops, which correlate well with clinical FFR measurements. These results validate the model's accuracy and reliability in clinical settings. The framework offers a structured approach to applying CFD in coronary artery disease diagnostics and treatment planning, confirming its effectiveness in improving diagnostic and therapeutic strategies. This study lays a strong foundation for future CFD-based research in cardiovascular interventions.

## ACKNOWLEDGEMENTS:

The authors would like to express their sincere gratitude to the Tertiary Education Trust Fund Nigeria (TETFund) for their financial support provided through Federal Polytechnic Bauchi, Nigeria, under research number TETF/DR&D/CE/POLY/BAUCHI/IBR/2024/VOL. FPTB-08.

## REFERENCES

- [1] C.A. Taylor, T.A. Fonte, J.K. Min, Computational fluid dynamics applied to cardiac computed tomography for noninvasive quantification of fractional flow reserve: scientific basis, *J. Am. Coll. Cardiol.* 61 (22) (2013) 2233–2241.
- [2] B.-K. Koo, A. Erglis, J.-H. Doh, D.V. Daniels, S. Jegere, H.-S. Kim, A. Dunning, T. DeFrance, A. Lansky, J. Leipsic, et al., Diagnostic of ischemia-causing coronary stenoses by noninvasive fractional flow reserve computed from coronary computed tomographic angiograms: results from the prospective multicenter DISCOVER-FLOW (diagnosis of ischemia-causing stenoses obtained via noninvasive fractional flow reserve) study, *J. Am. Coll. Cardiol.* 58 (19) (2011) 1989–1997.
- [3] J.K. Min, J. Leipsic, M.J. Pencina, D.S. Berman, B.-K. Koo, C. Van Mieghem, A. Erglis, F.Y. Lin, A.M. Dunning, P. Apruzzese, et al., Diagnostic accuracy of fractional flow reserve from anatomic CT angiography, *JAMA* 308 (12) (2012) 1237–1245.
- [4] B.L. Norgaard, J. Leipsic, S. Gaur, S. Seneviratne, B.S. Ko, H. Ito, J.M. Jensen, L. Mauri, B. De Bruyne, H. Bezerra, et al., Diagnostic performance of noninvasive fractional flow reserve derived from coronary computed tomography angiography in suspected coronary artery disease: the NXT trial (analysis of coronary blood flow using CT angiography: Next steps), *J. Am. Coll. Cardiol.* 63 (12) (2014) 1145–1155.
- [5] R.S. Driessen, I. Danad, W.J. Stuijffzand, P.G. Raijmakers, S.P. Schumacher, P.A. Van Diemen, J.A. Leipsic, J. Knuuti, S.R. Underwood, P.M. van de Ven, et al., Comparison of coronary computed tomography angiography, fractional flow reserve, and perfusion imaging for ischemia diagnosis, *J. Am. Coll. Cardiol.* 73 (2) (2019) 161–173.
- [6] P.S. Douglas, B. De Bruyne, G. Pontone, M.R. Patel, B.L. Norgaard, R.A. Byrne, N. Curzen, I. Purcell, M. Gutberlet, G. Rioufol, et al., 1-year outcomes of FFRCT-guided care in patients with suspected coronary disease: the PLATFORM study, *J. Am. Coll. Cardiol.* 68 (5) (2016) 435–445.
- [7] B. Norgaard, C. Terkelsen, O. Mathiassen, E. Grove, H. Botker, E. Parner, et al., Clinical outcomes using coronary CT angiography and FFRCT-guided management of stable chest pain patients, *J. Am. Coll. Cardiol.* 72 (18) (2018) 2123–2134.

Corresponding author: Mohammed Abdulhameed

✉ [amohd@fptb.edu.ng](mailto:amohd@fptb.edu.ng)

Department of Mathematics and Statistics, Federal Polytechnic Bauchi.

© 2024. Faculty of Technology Education. ATBU Bauchi. All rights reserved



- [8] M.A. Hlatky, B. De Bruyne, G. Pontone, M.R. Patel, B.L. Norgaard, R.A. Byrne, N. Curzen, I. Purcell, M. Gutberlet, G. Rioufol, et al., Quality-of-life and economic outcomes of assessing fractional flow reserve with computed tomography angiography: PLATFORM, *J. Am. Coll. Cardiol.* 66 (21) (2015) 2315–2323.
- [9] N. Curzen, Z. Nicholas, B. Stuart, S. Wilding, K. Hill, J. Shambrook, Z. Emlinton, D. Ball, C. Barrett, L. Johnson, et al., Fractional flow reserve derived from computed tomography coronary angiography in the assessment and management of stable chest pain: the FORECAST randomized trial, *Eur. Heart J.* 42 (37) (2021) 3844–3852.
- [10] S. Di Gregorio, M. Fedele, G. Pontone, A.F. Corno, P. Zunino, C. Vergara, A. Quarteroni, A computational model applied to myocardial perfusion in the human heart: From large coronaries to microvasculature, *J. Comput. Phys.* 424 (2021) 109836.
- [11] A. Updegrave, N.M. Wilson, J. Merkow, H. Lan, A.L. Marsden, S.C. Shadden, SimVascular: an open source pipeline for cardiovascular simulation, *Ann. Biomed. Eng.* 45 (2017) 525–541.
- [12] C.A. Taylor, C. Figueroa, Patient-specific modeling of cardiovascular mechanics, *Annu. Rev. Biomed. Eng.* 11 (2009) 109–134.
- [13] C.J. Arthurs, R. Khlebnikov, A. Melville, M. Marčan, A. Gomez, D. Dillon-Murphy, F. Cuomo, M. Silva Vieira, J. Schollenberger, S.R. Lynch, C. Tossas-Betancourt, K. Iyer, S. Hopper, E. Livingston, P. Youssefi, A. Noorani, S. Ben Ahmed, F.J.H. Nauta, T.M.J. van Bakel, Y. Ahmed, P.A.J. van Bakel, J. Mynard, P. Di Achille, H. Gharahi, K.D. Lau, V. Filonova, M. Aguirre, N. Nama, N. Xiao, S. Baek, K. Garikipati, O. Sahni, D. Nordsletten, C.A. Figueroa, CRIMSON: An open-source software framework for cardiovascular integrated modelling and simulation, *PLoS Comput. Biol.* 17 (5) (2021) e1008881.
- [14] A.M. Awad, K.S. Mekheimer, S.A. Elkilany, A.Z. Zaher, Leveraging elasticity of blood stenosis to detect the role of a non-Newtonian flow midst an arterial tube: mazumdar and Keller models, *Chin. J. Phys.* 77 (2022) 2520–2540.
- [15] K.S. Mekheimer, I. Shahzadi, S. Nadeem, A.M.A. Moawad, A.Z. Zaher, Reactivity of bifurcation angle and electroosmosis flow for hemodynamic flow through aortic bifurcation and stenotic wall with heat transfer, *Physica Scripta* 96 (1) (2021), 015216.
- [16] S.Y. Motlagh, S. Deyhim, Numerical study of magnetic drug targeting inside the bifurcated channel as a simplified model of right common iliac artery using Fe304-blood magnetic nanofluid, *Iranian J. Sci. Tech. Transact. Mech. Eng.* 47 (1) (2023) 51–65, <https://doi.org/10.1007/s40997-022-00507-y>.
- [17] F. He, X. Wang, L. Hua, T. Guo, Non-Newtonian effects of blood flow on hemodynamics in pulmonary stenosis: numerical simulation, *Appl. Bionics Biomech.* 2023 (2023), 1434832, <https://doi.org/10.1155/2023/1434832>.
- [18] K.K. Kolli, I. Arif, S.V. Peelukhana, P. Succop, L.H. Back, T.A. Helmy, M.A. Leesar, M.A. Effat, R.K. Banerjee, Diagnostic performance of pressure drop coefficient in relation to fractional flow reserve and coronary flow reserve, *J. Invasive Cardiol.* 26 (2014) 2–9.
- [19] S.V. Peelukhana, R.K. Banerjee, T.P. van de Hoef, K.K. Kolli, M. Effat, T. Helmy, M. Leesar, H. Kerr, J.J. Piek, P. Succop, L. Back, I. Arif, Evaluation of lesion flow coefficient for the detection of coronary artery disease in patient groups from two academic medical centers, *Cardiovasc. Revascularization Med.* 19 (3) (2018) 348–354.
- [20] L.C. Cheng, M.E. Clark, J.M. Robertson, Numerical calculations of oscillating flow in the vicinity of square wall obstacles in plane conduits, *J. Biomech.* 5 (1972) 467–484.
- [21] W. Liao, T. S Lee, H.T. Low, Numerical studies of physiological pulsatile flow through constricted tube, *Int. J. Numer.*

Corresponding author: Mohammed Abdulhameed

✉ [amohd@fptb.edu.ng](mailto:amohd@fptb.edu.ng)

Department of Mathematics and Statistics, Federal Polytechnic Bauchi.

© 2024. Faculty of Technology Education. ATBU Bauchi. All rights reserved



- Methods Heat Fluid Flow 14 (2004) 689–713.
- [22] P. Halder, A. Husain, M. Zunaid, A. Samad, Newtonian and Non-Newtonian pulsatile flows through an artery with stenosis, J. Eng. Res. 14 (2017) 191–205.
- [23] A. Razavi, E. Shirani, M.R. Sadeghi, Numerical simulation of blood pulsatile flow in a stenosed carotid artery using different rheological models, J. Biomech. 44 (2011) 2021–2030. [16] P. Youssefi, et al., Impact of patient-specific inflow velocity profile on hemodynamics of the thoracic aorta, J. Biomech. Eng. 140 (2018) 1–14.
- [24] M. Mahmoudi, A. Farghadan, D. McConnell, A.J. Barker, J.J. Wentzel, M.J. Budoff, A. Arzani, The story of wall shear stress in coronary artery atherosclerosis: biochemical transport and mechanotransduction, J. Biomech. Eng. 143 (2021), 041002.
- [25] M. Nagargoje, R. Gupta, Effect of asymmetry on the flow behavior in an idealized arterial bifurcation, Comput. Methods Biomech. Biomed. Eng. 23 (6) (2020) 232–247.
- [26] E. Lakzian, P. Akbarzadeh, Numerical investigation of unsteady pulsatile Newtonian/non-Newtonian blood flow through curved stenosed arteries, Bio Med. Mater. Eng. 30 (2019) 525–540.
- [27] Z. Abbas, M.S. Shabbir, N. Ali, Numerical study of magnetohydrodynamic pulsatile flow of sutterby fluid through an inclined overlapping arterial stenosis in the presence of periodic body acceleration, Results Phys. 9 (2018) 753–762.
- [28] COMSOL Multiphysics, Reference Manual, Version 5.2.

---

Corresponding author: Mohammed Abdulhameed

✉ [amohd@fptb.edu.ng](mailto:amohd@fptb.edu.ng)

Department of Mathematics and Statistics, Federal Polytechnic Bauchi.

© 2024. Faculty of Technology Education. ATBU Bauchi. All rights reserved